Pressure-Induced Crystallization and Characterization of the Tin Borate β-SnB_4O_7

Johanna S. Knyrim,[†] Falko M. Schappacher,[‡] Rainer Pöttgen,[‡] Jörn Schmedt auf der Günne,[†] Dirk Johrendt,[†] and Hubert Huppertz*,[†]

Department Chemie und Biochemie, Ludwig-Maximilians-Universität München, Butenandtstrasse 5-13, D-81377 München, Germany, and Institut für Anorganische und Analytische Chemie, Westfälische Wilhelms-Universität Münster, Corrensstrasse 30, D-48149 Münster, Germany

Received August 18, 2006. Revised Manuscript Received October 26, 2006

In the last years, several investigations were performed in the ternary system Sn−B−O as a simplified variant of the tin-based amorphous composite oxide (TCO), a material in use as negative electrode of lithium-ion rechargeable batteries. All compounds in this system are glasses, so the synthesis of crystalline approximands for a more detailed structural investigation would be favorable. The use of high-pressure/high-temperature conditions (7.5 GPa and 1100 °C; Walker-type multianvil apparatus) led to the synthesis of the first crystalline tin borate β-SnB_4O_7. The single-crystal structure determination of β-SnB_4O_7 showed $Pmn2_1$, $a = 1086.4(2)$ pm, $b = 444.80(9)$ pm, $c = 423.96(8)$ pm, $Z = 2$, $R_1 = 0.0155$, and $wR_2 = 0.0324$ (all data). In contrast to the isotypic phases MB_4O_7 (M = Sr, Pb, Eu, β-Ca, and β-Hg), the position of the tin atom in β-SnB_4O_7 is influenced by the existence of a stereochemically active lone pair. Furthermore, we report on thermoanalytical aspects (DTA-TG and temperature-resolved in situ powder diffraction), DFT calculations, IR spectroscopy, Mössbauer spectroscopic results, and solid-state NMR investigations on β-SnB_4O_7. The latter method allows us to make a general differentiation of Sn^{2+} and Sn^{4+} in Sn−O systems on the basis of well-separated $^{117/119}$Sn chemical shifts.

Introduction

In 1997, Idota et al. reported about a tin-based amorphous oxide that could replace the carbon-based lithium intercalation materials currently in use as the negative electrode of lithium-ion rechargeable batteries.[1] This tin-based amorphous composite oxide (TCO) has a complex composition $SnB_{0.56}P_{0.40}Al_{0.42}O_{3.6}$ and shows twice the gravimetry and four times the volumetric capacity of carbon-based materials. Unfortunately, this outstanding performance is counterbalanced by a large irreversible capacity, that is lost during the first electrochemical cycle. As the reasons are not yet fully understood, several groups tried to clarify the mechanisms at simplified variants of the TCO glasses. For example, Holland et al. investigated the borate anomaly of the Sn(II) environment in tin borate glasses of the general composition xSnO$(1-x)B_2O_3$, using ^{11}B and ^{119}Sn nuclear magnetic resonance (NMR) spectroscopies.[2] In this system, the introduction of SnO into the boroxol ring structure of B_2O_3 converts one symmetrically coordinated boroxol ring boron to a BO_4 tetrahedron, accompanied by changes in the environment of the neighboring threefold coordinated atoms. Due to the structural chemistry of Sn(II), which is dominated by the steric activity of a lone pair, trigonal pyramidal SnO_3 polyhedra can be found with the lone pair at one vertex, leading to a pseudo-tetrahedron. The authors showed that the increase in SnO leads to less symmetrical threefold-coordinated boron atoms, whereas the symmetry of the tin coordination becomes more axial.

Hayashi et al. investigated the structures of SnO−B_2O_3 glasses by various spectroscopic measurements, using solid-state NMR and X-ray photoelectron spectroscopy.[3] Additionally, they successfully prepared xSnO$(100-x)B_2O_3$ ($0 \leq x \leq 80$) glasses by mechanical milling.[4] These investigations showed that the composition dependence of T_g for the milled glasses was similar to that of the corresponding melt-quenched glasses.

Geijke et al. presented a neutron diffraction study of SnB_2O_4 glass, including a reverse Monte Carlo modeling, in which an average 3−3.5 fold coordination of boron gave an excellent agreement with the experimental structure factors.[5] Concerning SnO, the authors suggested more the role of a network glass former (bridging between two neighboring borate units) than simply as a network modifier. Another study on $SnB_{2.2}O_{4.3}$, using diffuse reflectance infrared spectroscopy, led to the conclusion that this compound is mainly built up from *meta*-borate groups forming a network.[6] Furthermore, Geijke et al. investigated the effect of lithium insertion/extraction in/out of SnB_2O_4 and $Sn_2B_3O_{6.5}$

* Corresponding author. E-mail: huh@cup.uni-muenchen.de.
† Ludwig-Maximilians-Universität München.
‡ Universität Münster.

(1) Idota, Y.; Kubota, T.; Matsufuji, A.; Maekawa, Y.; Miyasaka,T. *Science* **1997**, *276*, 1395−1397.
(2) Holland, D.; Smith, M. E.; Howes, A. P.; Davies, T.; Barrett, L. *Phys. Chem. Glasses* **2003**, *44* (2), 59−63.
(3) Hayashi, A.; Nakai, M.; Tatsumisago, M.; Minami, T.; Himei, Y.; Miura, Y.; Katada, M. *J. Non-Cryst. Solids* **2002**, *306*, 227−237.
(4) Hayashi, A.; Nakai, M.; Morimoto, H.; Minami, T.; Tatsumisago, M. *J. Mater. Sci.* **2004**, *39*, 5361−5364.
(5) Geijke, C.; Swenson, J.; Delaplané, R. G.; Börjesson, L. *Phys. Rev. B* **2002**, *65*, 212201−4.
(6) Geijke, C.; Zanghellini, E.; Svenson, J.; Börjesson, L. *J. Power Sources* **2003**, *119*−121, 576−580.

10.1021/cm061946w CCC: $37.00
Published on Web 12/23/2006

glass electrodes by in situ ^{119}Sn Mössbauer measurements.[7] They were able to show that there was some disruption of the glass network during the first cycle, which was responsible for a major part of the capacity loss.

Recapitulating, several investigations have been performed until now in the ternary system Sn−B−O as a simplified variant of the original TCO glass, in which all known compositions are glasses without any exception. Although glasses are only partly comparable to crystalline compounds, the knowledge about possible structural building blocks and models of linkage inside the glasses can be enhanced by crystalline approximands. Therefore, we started our investigations into the system Sn−B−O aiming at a crystalline tin borate by use of the parameter "pressure". In principle, pressure can induce amorphization or crystallization, depending on the applied parameters in a specific chemical system.[8−15] Several reasons for amorphization such as thermodynamic melting and mechanical instabilities were quoted. Meanwhile, it is established that the pressure-induced amorphization leads to a kinetically preferred amorphous state in most systems. The progress of the transformation to the high-pressure equilibrium state is presumably impeded by a lack of thermal energy. Recently, the assumption of an intermediate state between two thermodynamically stable states was confirmed by Zhang et al., showing that the final equilibrium phases are independent of the starting materials.[15] On the other hand, pressure can also induce crystallization of an amorphous compound by changing the Gibbs free energy. Especially in the borate systems, which often tend to form glasses, we were able to discover several new crystalline high-pressure polymorphs such as β-MB_4O_7 (M = Ca, Zn, Hg),[16−18] χ-$REBO_3$ (RE = Dy, Er),[19] ν-$DyBO_3$,[20] and new compositions such as, e.g., $RE_4B_6O_{15}$ (RE = Dy, Ho),[21−23] α-$RE_2B_4O_9$ (RE = Sm−Ho),[24−26] β-$RE_2B_4O_9$ (RE = Dy, Gd),[27,28] and $RE_3B_5O_{12}$ (RE = Tm−Lu),[29] whose successful syntheses were indispensably based on the "pressure" parameter. Now we could realize the first crystalline tin borate β-SnB_4O_7, of which we report the high-pressure synthesis, crystal structure, and properties herein. Because this tin borate represents a high-pressure phase, we assume the existence of a normal-pressure phase, that has been unknown until now. Therefore, we designated the presented high-pressure compound as "β-SnB_4O_7" and the unknown normal-pressure modification as "α-SnB_4O_7".

Experimental Section

Synthesis. According to eq 1, the starting materials for the synthesis of β-SnB_4O_7 were stoichiometric mixtures of B_2O_3 (Strem Chemicals, Newburyport, MA, 99.9%) and tin(II) oxide (Strem Chemicals, 99%).

$$SnO + 2B_2O_3 \xrightarrow[1100\ °C]{7.5\ GPa} \beta\text{-}SnB_4O_7 \quad (1)$$

They were compressed and heated in a multianvil assembly (18/11) with a modified Walker module (6−8 Kawai-type apparatus) and a 1000 t press (Voggenreiter, Mainleus, Germany). A precast MgO octahedron (Ceramic Substrates & Components, Isle of Wight, U.K.) with an edge length of 18 mm was used as a pressure medium. Eight tungsten carbide cubes (TSM 10, Ceratizit, Austria) with a truncation of 11 mm, separated by pyrophyllite gaskets, compressed the octahedron (18/11 assembly in conventional terminology). The mixture (∼65 mg) was filled into a cylindrical boron nitride crucible, that was sealed by a boron nitride plate. The sample cylinder was placed at the center of cylindrical resistance heaters (graphite), having a variably stepped wall thickness to minimize the thermal gradient along the sample. MgO rods filled the space on the top and bottom of the sample. Thermal insulation was provided by a cylindrical zirconia sleeve surrounding the furnace. The assembly was positioned inside the octahedron and made contact with a molybdenum plate at the top and a molybdenum plate at the bottom. The experimental temperature was monitored by means of a $Pt/Pt_{87}Rh_{13}$ thermocouple inserted axially into the octahedral assembly and with the hot junction being in contact with the boron nitride cylinder. Further details of the construction of the assembly can be found in the references.[30−35]

To synthesize β-SnB_4O_7, we compressed the assembly within 3 h to 7.5 GPa and heated it to 1100 °C in the following 10 min. After being held at this temperature for 5 min, the sample was cooled to 750 °C in another 15 min, and after that, cooled to room temperature within 1 min. After decompression, the recovered experimental octahedron was broken apart, and the sample was carefully separated from the surrounding hexagonal boron nitride. The air- and humidity-resistant compound β-SnB_4O_7 was obtained as a single-phase, coarsely crystalline, colorless solid.

All experiments at pressures beyond 7 GPa led exclusively to crystalline β-SnB_4O_7. Attempts to produce β-SnB_4O_7 as glass, using

(7) Geijke, C.; Nordström, E.; Fransson, L.; Edström, K.; Häggström, L.; Börjesson, L. *J. Mater. Chem.* **2002**, *12*, 2965−2970.
(8) Mishima, O.; Calvert, L. D.; Whalley, E. *Nature* **1984**, *310*, 393−395.
(9) Hemley, R. J.; Jephcoat, A. P.; Mao, H. K.; Ming, L. C.; Manghnani, M. H. *Nature* **1988**, *334*, 52−54.
(10) Deb, S. K.; Wilding, M.; Somayazulu, M.; McMillan, P. F. *Nature* **2001**, *414*, 528−530.
(11) Perottoni, C. A.; Da Jornada, H. A. H. *Science* **1997**, *280*, 886−889.
(12) Nguyen, J. H.; Kruger, M. B.; Jeanloz, R. *Phys. Rev. Lett.* **1997**, *78*, 1936−1939.
(13) Sharma, S. M.; Sikka, S. K. *Prog. Mater. Sci.* **1996**, *40*, 1−77.
(14) Ponyatovsky, E. G.; Barkalov, O. I. *Mater. Sci. Rep.* **1992**, *8*, 147−191.
(15) Zhang, J.; Zhao, Y.; Xu, H.; Zelinskas, M. V.; Wang, L.; Wang, Y.; Uchida, T. *Chem. Mater.* **2005**, *17*, 2817−2824.
(16) Huppertz, H. *Z. Naturforsch.* **2003**, *58b*, 257−265.
(17) Huppertz, H.; Heymann, G. *Solid State Sci.* **2003**, *5*, 281−289.
(18) Emme, H.; Weil, M.; Huppertz, H. *Z. Naturforsch.* **2005**, *60b*, 815−820.
(19) Huppertz, H.; von der Eltz, B.; Hoffmann, R.-D.; Piotrowski, H. *J. Solid State Chem.* **2002**, *166*, 203−212.
(20) Emme, H.; Huppertz, H. *Acta Crystallogr., Sect. C* **2004**, *60*, i117−i119.
(21) Huppertz, H.; von der Eltz, B. *J. Am. Chem. Soc.* **2002**, *124*, 9376−9377.
(22) Huppertz, H. *Z. Naturforsch.* **2003**, *58b*, 278−290.
(23) Huppertz, H.; Emme, H. *J. Phys.: Condens. Matter* **2004**, *16*, S1283−S1290.
(24) Emme, H.; Huppertz, H. *Z. Anorg. Allg. Chem.* **2002**, *628*, 2165.
(25) Emme, H.; Huppertz, H. *Chem.−Eur. J.* **2003**, *9*, 3623−3633.
(26) Emme, H.; Huppertz, H. *Acta Crystallogr., Sect. C* **2005**, *61*, i29−i31.
(27) Huppertz, H.; Altmannshofer, S.; Heymann, G. *J. Solid State Chem.* **2003**, *170*, 320−329.
(28) Emme, H.; Huppertz, H. *Acta Crystallogr., Sect. C* **2005**, *61*, i23−i24.
(29) Emme, H.; Valldor, M.; Pöttgen, R.; Huppertz, H. *Chem. Mater.* **2005**, *17*, 2707−2715.
(30) Huppertz, H. *Z. Naturforsch.* **2001**, *56b*, 697−703.
(31) Kawai, N.; Endo, S. *Rev. Sci. Instrum.* **1970**, *8*, 1178−1181.
(32) Walker, D.; Carpenter, M. A.; Hitch, C. M. *Am. Mineral.* **1990**, *75*, 1020−1028.
(33) Walker, D. *Am. Mineral.* **1991**, *76*, 1092−1100.
(34) Rubie, D. C. *Phase Transitions* **1999**, *68*, 431−451.
(35) Huppertz, H. *Z. Kristallogr.* **2004**, *219*, 330−338.

high cooling rates (quenching the assembly), did not succeed in any amorphous phase. The cooling rate in our high-pressure assembly was too low for the production of glass with the composition SnB_4O_7, as it was possible for other borates under these conditions. In contrast, experiments in the pressure range 1−2 GPa resulted only in amorphous phases. For example, the synthesis of SnB_4O_7, following eq 1 performed at a pressure of 1 GPa and a temperature of 650 °C and including a slow decrease in temperature (0.8 °C/min) to 350 °C, led to an X-ray amorphous product, that showed reflections of metallic tin, which originates from the reducing character of the hexagonal boron nitride capsule during long heating times. Moreover, the elongation of the reaction times destabilized the assemblies, resulting in distorted capsules in which an isolation of a product was difficult. Presumably, the destabilization occurred from a molten sample whose assembly stability was affected during long reaction times. Furthermore, we observed that a higher temperature (700 °C) at 1 GPa in combination with slow cooling rates caused an increasing in the amount of metallic tin in the product. Shortening the reaction time and lowering the temperature (heating to 500 °C in 6 min, followed by quenching) led to an amorphous phase as well. The differences between the products synthesized at 1−2 GPa and the crystalline phase β-SnB_4O_7 presented here will be discussed in the Results and Discussion.

Physical Measurements. *X-ray Diffraction.* Small single crystals of β-SnB_4O_7 were isolated by mechanical fragmentation and examined by Laue photographs. Single-crystal intensity data of β-SnB_4O_7 were measured with a STOE-IPDS I area detector diffractometer (Mo−K_α radiation (λ = 71.073 pm)). A numerical absorption correction was applied to the data. According to the systematic extinctions $h0l$ with $h + l \neq 2n$, $h00$ with $h \neq 2n$, and $00l$ with $l \neq 2n$, the space groups $Pmn2_1$ (No. 31) and $Pmnm$ (No. 59) were derived. The noncentrosymmetric group was found to be correct during the refinement. This was confirmed with the ADDSYM routine of the program PLATON.[36] Additionally, a powder sample of β-SnB_4O_7 was subjected to a qualitative powder SHG measurement, using the method reported by Kurtz & Perry.[37] The observed intensities of the second harmonic, generated by β-SnB_4O_7, signaled an SHG effect, thus corroborating the noncentrosymmetry of β-SnB_4O_7.[38]

Structure solution and parameter refinement (full-matrix least-squares against F^2) were successfully performed using the SHELX-97 software suite.[39] Details of the data collections and structure refinements are listed in Table 1. The positional parameters, anisotropic displacement parameters, interatomic distances, and interatomic angles are given in Tables 2−6.

The powder diffraction pattern was obtained from a 0.2 mm Mark capillary, filled with β-SnB_4O_7, using a STOE STADI P powder diffractometer with monochromatized Cu−$K_{\alpha1}$ radiation. The diffraction pattern was indexed with the program ITO[40] on the basis of an orthorhombic unit cell. The lattice parameters (Table 1) were calculated from least-squares fits of the powder data. The correct indexing of the pattern of β-SnB_4O_7 was confirmed by intensity calculations, taking the atomic positions from the structure refinement.[41] The lattice parameters, determined from the powder data, electron diffraction, and single-crystal data, tally well.

Table 1. Crystal Data and Structure Refinement for β-SnB_4O_7

empirical formula	SnB_4O_7
molar mass (g mol^{-1})	273.93
crystal system	orthorhombic
space group	$Pmn2_1$ (No. 31)
powder diffractometer	Stoe Stadi P
radiation	Cu $K_{\alpha1}$ (λ = 154.051 pm)
powder diffraction data	
a (pm)	1085.34(4)
b (pm)	444.84(3)
c (pm)	423.43(3)
V (nm^3)	0.2044(1)
single-crystal diffractometer	STOE IPDS I
radiation	Mo K_α (λ = 71.073 pm)
single-crystal data	
a (pm)	1086.4(2)
b (pm)	444.80(9)
c (pm)	423.96(8)
V (nm^3)	0.2049(1)
formula units per cell *Z*	2
T (K)	293(2)
calculated density (g cm^{-3})	4.44
crystal size (mm^3)	0.08 × 0.08 × 0.03
detector distance (mm)	40.0
exposure time per plate (min)	16.0
absorption coefficient (mm^{-1})	6.2
F(000)	252
θ range (deg)	4.6 to 28.7
range in *hkl*	±14, ±6, ±5
scan type	φ/ω
total no. of reflections	2027
no. of independent reflections	600 (R_{int} = 0.0218)
Flack parameter	0.00(3)
no. of reflections with $I > 2\sigma(I)$	581 (R_σ = 0.0182)
data/parameters	600/59
absorption correction	empirical
GOF (F^2)	1.064
final *R* indices [$I > 2\sigma$(I)]	R_1 = 0.0145, wR_2 = 0.0322
R indices (all data)	R_1 = 0.0155, wR_2 = 0.0324
extinction coefficient	0.019(2)
largest diff. peak and hole (e Å^{-3})	0.763/−0.550

Table 2. Atomic Coordinates and Isotropic Equivalent Displacement Parameters U_{eq}[a] (Å^2) for β-SnB_4O_7 (space group $Pmn2_1$)[a]

atom	Wyckoff position	*x*	*y*	*z*	U_{eq}
Sn1	2*a*	0	0.82402(5)	0.89554(5)	0.0086(2)
B1	4*b*	0.1225(3)	0.3272(6)	0.444(2)	0.004(2)
B2	4*b*	0.2481(3)	0.1749(6)	0.9742(7)	0.0022(6)
O1	4*b*	0.2197(2)	0.1298(4)	0.6188(5)	0.0032(4)
O2	4*b*	0.1422(2)	0.6426(4)	0.5237(5)	0.0042(4)
O3	4*b*	0.1372(2)	0.2733(5)	0.1116(5)	0.0040(4)
O4	2*a*	0	0.2309(6)	0.5541(6)	0.0029(5)

[a] U_{eq} is defined as one-third of the trace of the orthogonalized U_{ij} tensor.

Table 3. Anisotropic Displacement Parameters (Å^2) for β-SnB_4O_7 (space group $Pmn2_1$)

atom	U_{11}	U_{22}	U_{33}	U_{23}	U_{13}	U_{12}
Sn1	0.0075(2)	0.0116(2)	0.0066(2)	0.0016(2)	0	0
B1	0.004(2)	0.0019(9)	0.006(4)	−0.000(2)	−0.001(2)	−0.0003(9)
B2	0.004(2)	0.002(2)	0.000(2)	0.0000(8)	0.0001(8)	0.000(2)
O1	0.005(2)	0.0021(8)	0.0022(8)	−0.0002(7)	−0.0010(8)	0.0015(7)
O2	0.005(2)	0.0025(8)	0.0051(7)	−0.0009(7)	0.0010(7)	0.0005(7)
O3	0.004(2)	0.0053(8)	0.0024(9)	−0.0010(6)	−0.0005(7)	0.0015(7)
O4	0.002(2)	0.003(2)	0.004(2)	0.0028(9)	0	0

Temperature-dependent X-ray powder diffraction experiments were performed on a STOE Stadi P powder diffractometer (Mo−K_α) with a computer controlled STOE furnace: The sample was enclosed in a quartz capillary and heated from room temperature to 500 °C in 100 °C steps and from 500 to 1100 °C in 50 °C steps. Afterwards, the sample was cooled to 500 °C in 50 °C steps, and below 500 °C in 100 °C steps. At each temperature, a diffraction pattern was recorded over the angular range $7° \leq 2\theta \leq 22°$.

(36) Spek, A. L. *PLATON A Multipurpose Crystallographic Tool*; Utrecht University: Utrecht, The Netherlands, 2002.
(37) Kurtz, S. K.; Perry, T. T. *J. Appl. Phys.* **1968**, *39*, 3798−3813.
(38) Becker, P. 2006, private communication.
(39) Sheldrick, G. M. *SHELXS97 and SHELXL97 Program Suite for the Solution and Refinement of Crystal Structures*; University of Göttingen, Germany, **1997**.
(40) Visser, J. W. *J. Appl. Crystallogr.* **1969**, *2*, 89−95.
(41) *WinX^{POW} Software*; STOE & CIE GmbH: Darmstadt, Germany, 1998.

Table 4. Interatomic B−O Distances (pm) Calculated with the Single-Crystal Lattice Parameters in β-SnB_4O_7 (standard deviations in parentheses)

B1−O3	143.6(4)	B2−O3	140.8(4)	O1−B2a	152.8(4)
B1−O2	145.9(3)	B2−O2	145.7(4)	O1−B2b	155.1(4)
B1−O4	147.5(4)	B2−O1a	152.8(4)	O1−B1	156.1(4)
B1−O1	156.1(4)	B2−O1b	155.1(4)		∅ 154.7[a]
	∅ 148.3[a]		∅ 148.6[a]		

[a] ∅ over all distances = 148.4.

Table 5. Interatomic Sn−O Distances (pm) Calculated with the Single-Crystal Lattice Parameters in β-SnB_4O_7 (standard deviations in parentheses)

Sn1−O4a	231.8(3)
Sn1−O2	235.0(2) × 2
Sn1−O3a	265.6(2) × 2
Sn1−O1	298.7(2) × 2
Sn1−O4b	300.9(3)
Sn1−O3b	301.0(2) × 2

Table 6. Interatomic Angles (deg) Calculated with the Single-Crystal Lattice Parameters in β-SnB_4O_7 (standard deviations in parentheses)

O4−B1−O1	107.2(3)	O2−B2−O1a	104.4(2)	B2a−O1−B2b	117.3(2)
O3−B1−O1	107.3(2)	O3−B2−O1b	105.8(2)	B2a−O1−B1	117.6(2)
O2−B1−O1	109.3(3)	O3−B2−O1a	107.8(2)	B2b−O1−B1	121.6(2)
O2−B1−O4	109.7(3)	O1a−B2−O1b	108.7(2)		∅118.8
O3−B1−O4	111.3(3)	O2−B2−O1b	112.0(2)		
O3−B1−O2	111.9(3)	O3−B2−O2	117.8(2)		
	∅109.5		∅109.4		

Thermoanalytical Investigations. The DTA-TG curve of β-SnB_4O_7 was recorded between room temperature and 600 °C with a heating rate of 10 °C min^{-1}, using a Setaram TGA 92−2400 combined DTA-TG thermobalance.

Vibrational Spectroscopy. A FTIR spectrum of β-SnB_4O_7 was obtained at room temperature using a Bruker IFS 66v/S spectrometer with DTGS detector. The sample was thoroughly mixed with dried KBr (5 mg of the sample, 500 mg of KBr). The preparation procedure was performed in a glovebox under a dried argon atmosphere. The spectrum was collected in a range from 400 to 4000 cm^{-1} with a resolution of 2 cm^{-1}. During the measurement, the sample chamber was evacuated.

Mössbauer Spectroscopy. A $Ca^{119}SnO_3$ source was available for the ^{119}Sn Mössbauer spectroscopic investigations. The sample (diluted with α-quartz) was placed into a thin-walled PVC container at a content between 10 and 15 mg Sn/cm^2. A palladium foil of 0.05 mm thickness was used to reduce the tin K X-rays, concurrently emitted by this source. The measurements were conducted in the usual transmission geometry at 77 K and room temperature.

Solid-State NMR. The NMR experiments on β-SnB_4O_7 were carried out on a BRUKER Avance DSX spectrometer, equipped with commercial 2.5 mm and 4 mm MAS NMR probes. The magnetic field strength was 11.75 T, corresponding to ^{117}Sn and ^{11}B resonance frequencies of 178.03 and 160.50 MHz, respectively. A commercially available pneumatic control unit was used to limit MAS frequency variations to a 2 Hz interval during the experiment. Samples were spun at 10 and 25 kHz, respectively. The chemical shift values refer to $Sn(CH_3)_4$ and $BF_3{\cdot}Et_2O$ as external chemical shift references for ^{117}Sn and ^{11}B. The repetition rates of the experiments were 300 and 50 s, respectively. The ^{117}Sn MAS spectrum was obtained from 200 accumulated transients. The ^{11}B MQMAS was obtained using a triple-quantum 3 pulse sequence with a z-filter.[42] The SOQE parameters and isotropic chemical shift values were determined from the moment analysis[42,43] of the sheared MQMAS spectrum.

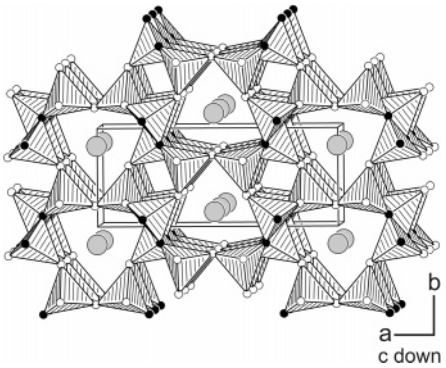

Figure 1. Crystal structure of β-SnB_4O_7; view along [001]. Grey spheres represent Sn cations, white spheres show twofold oxygen atoms ($O^{[2]}$), and black spheres show threefold oxygen atoms ($O^{[3]}$).

Simulations of the ^{117}Sn chemical shift parameters were done by minimizing the squared difference between experiment and simulation, using the SIMPSON MINUIT routines,[44] and the chemical shift conventions implemented in SIMPSON.[45]

DFT Calculations. Self-consistent DFT band structure calculations were performed by the LMTO-method in its scalar-relativistic version (program TB-LMTO-ASA). Detailed descriptions are given elsewhere.[46,47] Reciprocal space integrations were performed with the tetrahedron method,[48] using 273 irreducible *k*-points. The basis set consisted of Sn-5s/5p/{5d/4f}, B-2s/2p{3d}, and O-{3s}2p{3d}. Orbitals given in parenthesis were downfolded.[49] To achieve space filling within the atomic sphere approximation, we introduced interstitial spheres. A three-dimensional grid of the charge density and the electron localization function (ELF)[50,51] were calculated. In the density functional theory, ELF depends on the excess of local kinetic energy due to the Pauli principle as compared to a bosonic system. High values of ELF appear in regions of space where the Pauli principle does not increase the local kinetic energy and thus pairing of electrons plays an important role. These regions can be assigned either to covalent bonds or to lone pairs.

Results and Dicussion

Crystal Structure. β-SnB_4O_7 consists exclusively of corner-sharing BO_4 tetrahedra, being isotypic to the known high-pressure phases β-CaB_4O_7[16] and β-HgB_4O_7[18] as well as to the ambient pressure phases SrB_4O_7,[52,53] PbB_4O_7,[53,54] and EuB_4O_7.[55] Figure 1 shows the crystal structure of β-SnB_4O_7 along [001] exhibiting a network of corner-sharing BO_4 tetrahedra and forming channels along [001], that are

(42) Amoureux, J.-P.; Fernandez, C.; Steuernagel, S. *J. Magn. Reson.* **1996**, *A123*, 116−118.
(43) Herreros, B.; Metz, A. W.; Harbison, G. S. *Solid State Nucl. Magn. Reson.* **2000**, *16*, 141−150.
(44) Vosegaard, T.; Malmendal, A.; Nielsen, N. C. *Monatsh. Chem.* **2002**, *133*, 1555−1574.
(45) Bak, M.; Rasmussen, J. T.; Nielsen, N. C. *J. Magn. Reson.* **2000**, *147*, 296−330.
(46) Andersen, O. K.; Jepsen, O. *Tight-Binding LMTO 4.7c*; Max-Planck-Institut für Festkörperforschung: Stuttgart, Germany, 1994.
(47) Andersen, O. K.; Jepsen, O.; Sob, M. In *Electronic Band Structure and its Applications*, *Lect. Notes Phys.* Yussouff, M., Ed.; Springer-Verlag: Berlin, 1987; Vol. 283.
(48) Blöchl, P. E.; Jepsen, O.; Andersen, O. K. *Phys. Rev. B* **1994**, *49*, 16223−16233.
(49) Lambrecht, W. R. L.; Andersen, O. K. *Phys. Rev. B* **1986**, *34*, 2439−2449.
(50) Silvi, B.; Savin, A. *Nature* **1994**, *371*, 683−686.
(51) Becke, A. D.; Edgecomb, K. E. *J. Chem. Phys.* **1990**, *92*, 5397−5403.
(52) Pan, F.; Shen, G.; Wang, R.; Wang, X.; Shen, D. *J. Cryst. Growth* **2002**, *241*, 108−114.
(53) Perloff, A.; Block, S. *Acta Crystallogr.* **1966**, *20*, 274−279.
(54) Corker, D. L.; Glazer, A. M. *Acta Crystallogr., Sect. B* **1996**, *52*, 260−265.
(55) Machida, K.-I.; Adachi, G.-Y.; Shiokawa, J. *Acta Crystallogr., Sect. B* **1980**, *36*, 2008−2011.

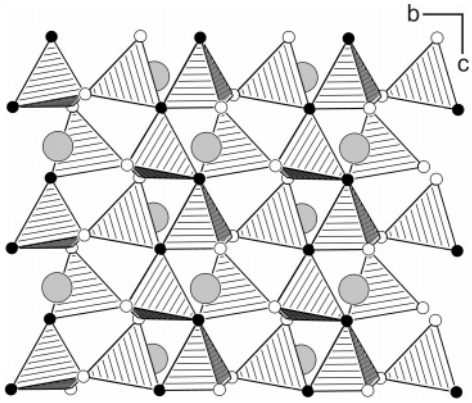

Figure 2. Crystal structure of β-SnB_4O_7; view along [$\bar{1}$00]. Grey spheres show tin cations, white spheres represent $O^{[2]}$ coordinated oxygen atoms, and dark spheres represent $O^{[3]}$ coordinated oxygen atoms.

built from four- and six-membered rings. The tin cations lie in the six-membered ring channels, whereas the four-membered ring channels remain empty. Figure 2 illustrates the highly condensed layers along [$\bar{1}$00] partially built up by three coordinate oxygen atoms $O^{[3]}$ (black spheres), which are also found in a few other borates, e.g., β-ZnB_4O_7,[17] β-$RE(BO_2)_3$ (RE = Tb−Lu),[56,57] γ-$RE(BO_2)_3$ (RE = La−Nd),[58,59] and minerals such as tunnelite ($SrB_6O_9(OH)_2 \cdot 3\ H_2O$),[60] strontioginorite ($(Sr,Ca)_2B_{14}O_{20}(OH)_6 \cdot 6\ H_2O$),[61] aristarainite ($Na_2Mg[B_6O_8(OH)_4]_2 \cdot 4\ H_2O$),[62] and the high-pressure modification of B_2O_3[63] itself. Figure 2 shows clearly that all tetrahedra point toward the $-c$ direction, confirming the noncentrosymmetric structure of β-SnB_4O_7.

The B−O bond lengths in β-SnB_4O_7 (Table 4) vary between 141 and 156 pm, with an average B−O bond length of 148.5 pm, which is slightly larger than the known average value of 147.0 pm for borates.[64,65] As expected, the bonds to three-coordinated oxygen atoms $O^{[3]}$ are significantly longer (153−156 pm) than the average, with partial compensation by the shortening of other bonds. Longer bonds can also be found in the borates MB_4O_7 (M = Sr, Pb, Eu)[52−55] and β-MB_4O_7 (M = Ca, Hg),[16−18] as well as in β-ZnB_4O_7[17] (Table 8). The O−B−O angles in the two crystallographically independent BO_4 tetrahedra vary between 104.4 and 117.8° (Table 6). These strong deviations from the ideal tetrahedron angle are not exceptional for borates, synthesized under extreme conditions. Examples for such strongly distorted tetrahedra in BO_4 networks can be found, e.g., in the high-pressure phases α-$RE_2B_4O_9$ (RE = Eu−Tb) with

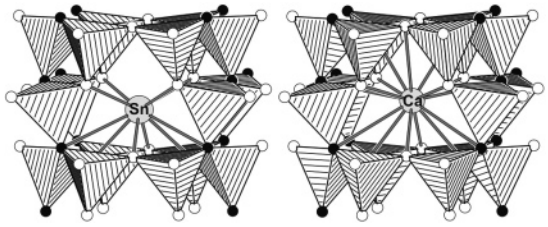

Figure 3. Coordination sphere of tin in the crystal structure of β-SnB_4O_7 with the sterically active lone pair of Sn^{2+} (left) compared to the coordination sphere of Ca^{2+} in the crystal structure of β-CaB_4O_7 (right).

Table 7. Charge Distribution in β-SnB_4O_7 Calculated with the Bond-Length/Bond-Strength Concept (ΣV)[74,75] and the Chardi Concept (ΣQ)[76]

	Sn1	B1	B2	O1	O2	O3	O4
ΣV	1.79	2.98	2.97	−1.93	−1.95	−1.97	−1.98
ΣQ	1.90	2.95	3.09	−1.70	−2.14	−2.12	−2.09

Table 8. Average Interatomic B−$O^{[3]}$ Distances (pm) of β-SnB_4O_7 in Comparison to the B−$O^{[3]}$ Distances (pm) in the Isotypic Phases MB_4O_7 (M = Sr, Pb, Eu) and β-MB_4O_7 (M = Ca, Hg) as well as in β-ZnB_4O_7.

compd	avg B−$O^{[3]}$ distance
SrB_4O_7	155.0
PbB_4O_7	155.4
EuB_4O_7	154.4
β-HgB_4O_7	152.7
β-CaB_4O_7	153.7
β-SnB_4O_7	154.7
β-ZnB_4O_7	155.3

O−B−O angles varying between 99.5 and 118.9° for α-$Eu_2B_4O_9$, 99.4−119.0° for α-$Gd_2B_4O_9$, and 99.4−119.4° for α-$Tb_2B_4O_9$.[22−24] The B−$O^{[3]}$−B angles inside the OB_3 group are 117.3, 117.6, and 121.6°, with a mean value of 118.8° (Table 6). The slight distortion of the OB_3 group is understandable, because the Sn^{2+} ions lie in the direct neighborhood of the OB_3 group with an $O^{[3]}$−Sn distance of 298.7 pm (Table 5). The coordinative contribution of the $O^{[3]}$ leads to a deflection of these atoms from the plane into the direction of the Sn^{2+} ions. Similar distortions inside the $O^{[3]}B_3$ group can be found in other borates, e.g., β-ZnB_4O_7,[17] β-CaB_4O_7,[16] and β-HgB_4O_7.[18]

In contrast to the isotypic phases β-CaB_4O_7[16] and β-HgB_4O_7,[18] where the M^{2+} ions are coordinated by 15 oxygen atoms (β-CaB_4O_7, 242−316 pm; β-HgB_4O_7, 237−315 pm), the coordination number in β-SnB_4O_7 can be described as a 10 + 5 coordination (see Figure 3). The Sn−O distances vary between 232 and 301 pm for the 10 nearest oxygen atoms (Table 5). Five oxygen atoms can be found in a distance of 318 pm (2×), 320 pm (2×), and 333 pm that make only a negligible coordinative contribution to the Sn^{2+} ion. ECoN calculations (effective coordination numbers according to Hoppe)[66−68] for the Sn^{2+} ions confirm the coordination number of 10 in β-SnB_4O_7, if values of δ-ECoN smaller than 0.05 are neglected. The reason for the different coordination of the Sn^{2+} ions compared to the Ca^{2+} and Hg^{2+} ions may be the sterically active lone pair localized at Sn^{2+}.

(56) Emme, H.; Nikelski, T.; Schleid, Th.; Pöttgen, R.; Möller, M. H.; Huppertz, H. *Z. Naturforsch.* **2004**, *59b*, 202−215.
(57) Nikelski, T.; Schleid, Th. *Z. Anorg. Allg. Chem.* **2003**, *629*, 1017−1022.
(58) Emme, H.; Despotopoulou, C.; Huppertz, H. *Z. Anorg. Allg. Chem.* **2004**, *630*, 1717.
(59) Emme, H.; Despotopoulou, C.; Huppertz, H. *Z. Anorg. Allg. Chem.* **2004**, *630*, 2450−2457.
(60) Clark, J. R. *Am. Mineral.* **1964**, *49*, 1549−1568.
(61) Konnert, J. A.; Clark, J. R.; Christ, C. L. *Am. Mineral.* **1970**, *55*, 1911−1931.
(62) Ghose, S.; Wan, C. *Am. Mineral.* **1977**, *62*, 979−989.
(63) Prewitt, C. T.; Shannon, R. D. *Acta Crystallogr., Sect. B* **1968**, *24*, 869−874.
(64) Hawthorne, F. C.; Burns, P. C.; Grice, J. D. Reviews in Mineralogy. In *Boron: Mineralogy, Petrology, and Geochemistry*; Mineralogical Society of America: Washington, D.C., 1996; Chapter 2, Vol. 33.
(65) Zobetz, E. *Z. Kristallogr.* **1990**, *191*, 45−57.
(66) Hoppe, R. *Angew. Chem.* **1966**, *78*, 52−63; *Angew. Chem., Int. Ed.* **1966**, *5*, 96−106.
(67) Hoppe, R. *Angew. Chem.* **1970**, *82*, 7−16; *Angew. Chem., Int. Ed.* **1970**, *9*, 25−34.
(68) Hübenthal, R. *MAPLE Program for the Calculation of MAPLE Values*, version 4; University of Giessen: Giessen, Germany, 1993.

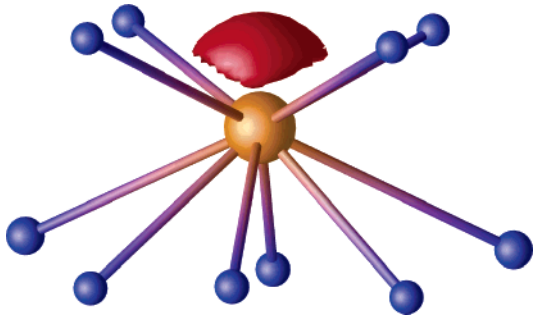

Figure 4. The lone pair at the Sn^{2+} ion in β-SnB_4O_7 visualized by the electron localization function (ELF) (isosurface value ELF = 0.93).

Bohatý et al. presented a detailed comparison of the coordination surroundings of Pb^{2+} and Sr^{2+} ions in PbB_4O_7 and SrB_4O_7, respectively.[69] The comparison signaled a slightly off-center shift of Pb^{2+} within its coordination surrounding compared to Sr^{2+}, caused by a moderate influence of the lone pair, which is present in PbB_4O_7. This effect is much stronger in β-SnB_4O_7.

To analyze the conspicuous lone pair behavior of PbB_4O_7 and β-SnB_4O_7, we have calculated the band structure of both compounds and the electron density distribution of β-SnB_4O_7. The electron localization function ELF is a useful tool to discover regions with paired spins, as expected for covalent bonds or lone pairs. Figure 4 displays the coordination of the tin atoms in β-SnB_4O_7, decorated with an ELF isosurface of ELF = 0.93. The lone pair at the tin atom is clearly visible and points towards the "empty" space above the tin atom. Thus, the DFT calculations support the existence of the stereochemically active lone pair of Sn^{2+} in β-SnB_4O_7, but it is not yet clear why the isostructural lead compound shows no distinctive asymmetry, as reported in ref 69. In recently published papers,[70,71] it is shown that the reason for lone pair formation in tin- and lead-chalcogenides mainly lies in the antibonding Sn(5s)−O(2p) interactions, which decrease the energy separation of the Sn(5s)−Sn(5p) states and allow s−p mixing. So, the more s−p mixed levels, that occur near the Fermi energy (ϵ_F), the stronger the tendency to form a lone pair at the tin (or lead) site. Figure 5 shows the partial density-of-states (PDOS) for the s and p orbitals of Sn in β-SnB_4O_7, Pb in PbB_4O_7 with off-center Pb (structure of β-SnB_4O_7), and finally Pb in the experimental structure with a nearly symmetric environment.[72] Strong s orbital contributions discern between ϵ_F and −2 eV for β-SnB_4O_7, which are significantly reduced by ∼25% in "PbB_4O_7" with the same structure. These s levels mix with p orbitals (dotted lines) in the same energy range and form the lone pair at the tin or lead site. But this tendency is much stronger in the tin compound than in PbB_4O_7. The lead atoms in the experimental structure of PbB_4O_7 are much more symmetrically coordinated. Consequently, the s−p contribution near ϵ_F is very low (upper part of Figure 5), and almost no indication of lone pair formation is discernible in the PDOS

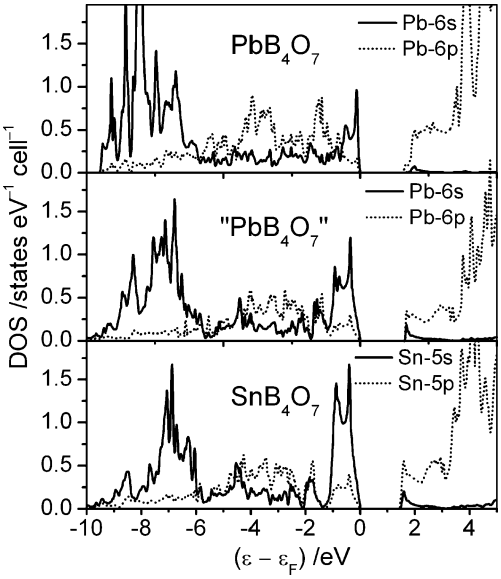

Figure 5. Partial densitiy-of-states (PDOS) diagrams of s and p orbitals in β-SnB_4O_7 (bottom), "PbB_4O_7" with β-SnB_4O_7 structure (middle), and experimental PbB_4O_7 (top).

of PbB_4O_7, in agreement with the experimental data. Our analysis supports the conclusion drawn in ref 71 that the lone pair is not a result of chemically inert s orbitals (equally present in Sn^{2+} and Pb^{2+}) but relies on the electronic interaction with the coordinated anions. Thus, the asymmetric oxygen coordination drives to the formation of the lone pair, and vice versa. The unit-cell volumes of β-SnB_4O_7 and PbB_4O_7 differ by only 0.3%, and the available space for Sn^{2+} and Pb^{2+} within the coordination polyhedra is almost the same. But the ionic radius[73] for Pb^{2+} (1.29 Å) is larger than that for Sn^{2+} (1.22 Å). Therefore, lead is well-coordinated (almost) in the center of the oxygen polyhedron, but the smaller tin ion shifts significantly off-center, so the lone pair results from this asymmetric oxygen environment.

Additionally, we calculated bond-valence sums for β-SnB_4O_7 with the bond-length/bond-strength (ΣV) and CHARDI concepts (ΣQ) (Table 7).[74−76] For bond-valence parameters for the bond-length/bond-strength concept, we used R_{ij} = 137.1 for B−O bonds and R_{ij} = 198.4 for Sn−O bonds.[75] The formal ionic charges of the atoms, acquired by X-ray structure analysis, were in agreement within the limits of the concepts, except the threefold coordinated oxygen atom O1, which shows a reduced value of −1.70 (ΣQ) in the CHARDI concept. Similar deviating values for the $O^{[3]}$ atoms are obtained in β-CaB_4O_7 (−1.92 (ΣV); −1.77 (ΣQ))[16], β-HgB_4O_7 (−2.06 (ΣV); −1.83 (ΣQ)),[18] and β-ZnB_4O_7 (−1.83 (ΣV); −1.67 (ΣQ)).[17] Remarkably, in all these cases, the deviation was only observed in the CHARDI calculations (ΣQ), whereas the bond-length/bond-strength values (ΣV) corresponded to the expected values. We then calculated the MAPLE values (Madelung part of lattice energy)[66−68] for

(69) Bohatý, L.; Haussühl, S.; Liebertz, J.; Becker, P.; Stein, W.-D.; Braden, M. *Z. Kristallogr. Suppl.* **2006**, 93.
(70) Walsh, A.; Watson, G. W. *J. Phys. Chem. B* **2005**, *109*, 18868−18875.
(71) Walsh, A.; Watson, G. W. *J. Solid State Chem.* **2005**, *178*, 1422−1428.
(72) Perloff, A.; Block, S. *Acta Crystallogr.* **1965**, *20*, 274−279.
(73) Shannon, R. D.; Prewitt, C. T. *Acta Crystallogr., Sect. B* **1969**, *25*, 925−946.
(74) Brown, I. D.; Altermatt, D. *Acta Crystallogr., Sect. B* **1985**, *41*, 244−247.
(75) Brese, N. E.; O'Keeffe, M. *Acta Crystallogr., Sect. B* **1991**, *47*, 192−197.
(76) Hoppe, R.; Voigt, S.; Glaum, H.; Kissel, J.; Müller, H. P.; Bernet, K. *J. Less-Common Met.* **1989**, *156*, 105−122.

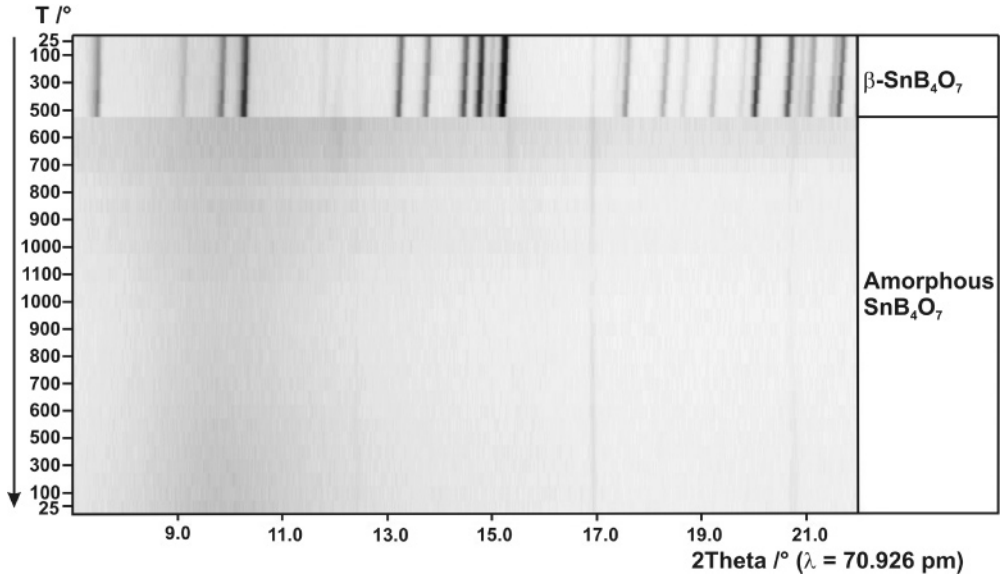

Figure 6. Temperature-dependent X-ray powder patterns, following the decomposition of β-SnB_4O_7.

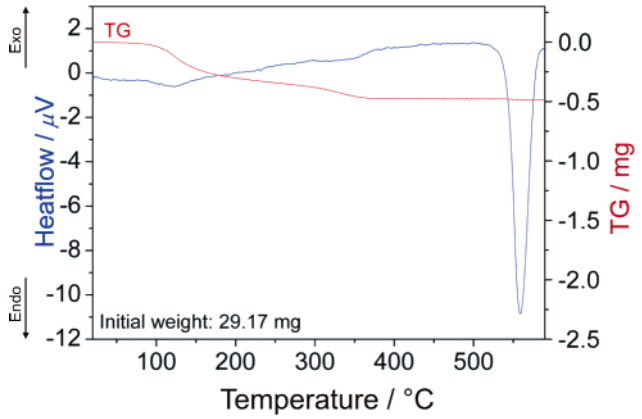

Figure 7. Differential thermal analysis curve and thermogravimetric curve of β-SnB_4O_7.

β-SnB_4O_7 to compare them with MAPLE values of the binary components, SnO, and the high-pressure modification B_2O_3-(II). Their foundation therefore is the additive potential of the MAPLE values, by which it is possible to calculate hypothetical values for β-SnB_4O_7, starting from the binary oxides. For β-SnB_4O_7 we obtained a value of 47755 kJ/mol in comparison to 47638 kJ/mol (deviation: 0.2%) starting from the binary oxides (1 × SnO (3762 kJ/mol + 2 × B_2O_3-(II) (21938 kJ/mol)).

Thermal Behavior. Different thermoanalytical investigations were performed to study the high-temperature stability and the metastable character of β-SnB_4O_7. Figure 6 illustrates the temperature-dependent X-ray powder diffraction patterns of β-SnB_4O_7, showing a transformation of the high-pressure phase into an X-ray amorphous phase after successive heating to 500−550 °C, referring to the loss of long-range order in the crystalline state. These results are in agreement with the DTA measurements, performed between room temperature and 600 °C (Figure 7). During the heating of β-SnB_4O_7, a broad endothermic effect occurred in the DTA between 520 and 580 °C that was due to a melting process of the compound. A small weight loss (2%) could be observed in the thermogravimetrical measurement between 100 and 350 °C that could be attributed to a loss of water and boric acid.

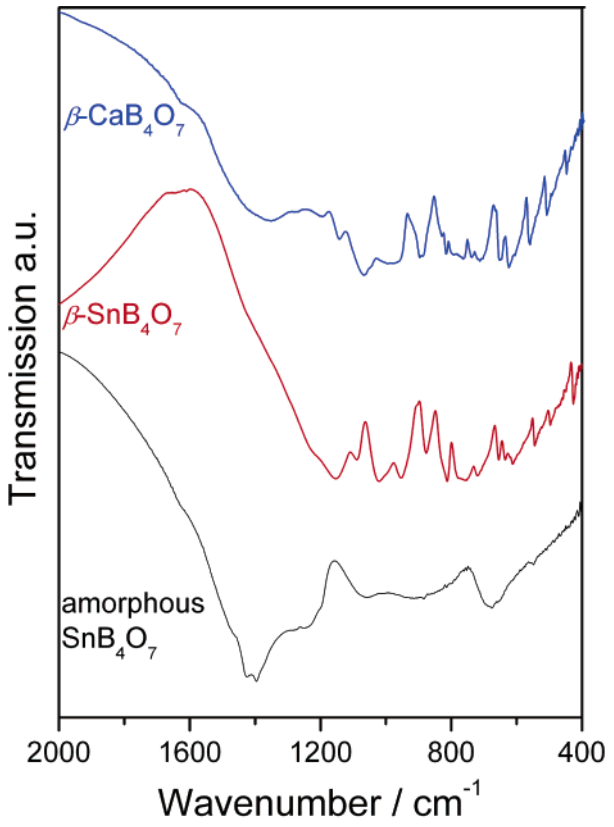

Figure 8. Infrared spectra of β-CaB_4O_7, β-SnB_4O_7, and amorphous SnB_4O_7.

The temperature-dependent X-ray powder diffraction patterns (Figure 6) showed that further heating to 1100 °C and subsequent cooling to room temperature did not succeed in obtaining any crystalline phase under ambient pressure conditions.

Vibrational Spectroscopic Characterization. Figure 8 shows the section 400−2000 cm^{-1} of the infrared spectrum of β-SnB_4O_7 (middle) in comparison with the spectra of the isotypic high-pressure phase β-CaB_4O_7 (top) and the amorphous ambient-pressure tin borate SnB_4O_7 (bottom). A first comparison of the three spectra confirms that β-SnB_4O_7 is isotypic to β-CaB_4O_7, as the absorptions of both compounds

are nearly identical. In contrast, the spectrum of the amorphous ambient-pressure phase SnB_4O_7 is completely different. In the spectra of β-SnB_4O_7 and β-CaB_4O_7, the absorption peaks between 800 and 1100 cm^{-1} are those typical for the tetrahedral borate group BO_4 as in YBO_3, $GdBO_3$, or $TaBO_4$.[77−79] Between 1100 and 1450 cm^{-1} and below 800 cm^{-1}, we observe absorptions typical for triangular BO_3 groups as in $LaBO_3$[80,81] and $Eu_2B_4O_9$.[82] Because BO_3 groups are missing in β-SnB_4O_7, the absorptions can be assigned to the corresponding OB_3 vibrations. Analogous geometrics and similar force parameters in the OB_3 group recommend this assignment, because it is also valid, for examples, for β-ZnB_4O_7,[17] β-CaB_4O_7,[16] and the high-pressure phase B_2O_3(II).[17,63] The existence of two crystallographically independent BO_4 units in the network structure of β-SnB_4O_7 in combination with OB_3 groups renders a detailed assignment of the broad bands difficult. The spectrum of the amorphous SnB_4O_7 exhibits a strong absorption around 1400 cm^{-1}, which is typical for BO_3 groups in borates. Around 1000 cm^{-1}, also characteristic BO_4 absorption bands can be observed. From these results, we conclude that the amorphous ambient-pressure phase SnB_4O_7 exhibits BO_3 and BO_4 groups in contrast to its high-pressure modification. Moreover, absorptions in the range 3100−3600 cm^{-1} show the presence of OH^-/H_2O, indicating that there is no pure SnB_4O_7. Up to now, it has not been possible to synthesize a defined, reproduceable composition SnB_4O_7.

Mössbauer Spectroscopy. The ^{119}Sn Mössbauer spectroscopy is a sensitive tool for investigating the coordination environment of tin in tin borate glasses. The spectra of β-SnB_4O_7 at 77 K and room temperature are presented in Figure 9, together with transmission integral fits. The fitting parameters are listed in Table 9. Both spectra show a main signal at an isomer shift of 4.09(1) mm/s and a line width of 0.88(1) mm/s, compatible with divalent tin. A small impurity component (ca. 5% of the total area) around 0 mm/s results most likely from a minor SnO_2 content[83] of the sample. Because of the low site symmetry of the tin site (*m*), the spectra show quadrupole splitting of 0.71(3) and 0.78(3) mm/s at room temperature and 77 K, respectively.

It is worthwhile to note that the ^{119}Sn Mössbauer spectrum of a SnB_2O_4 glass[7] shows a smaller isomer shift (between 3.09 and 3.17 mm/s) and a much higher quadrupole splitting parameter, clearly indicating different tin coordinations in the SnB_2O_4 glass than in the crystalline material β-SnB_4O_7.

Solid-State NMR Investigations. In agreement with the diffraction results, one tin and two boron positions were resolved in the solid-state NMR experiments. The ^{117}Sn chemical shift parameters were $\delta_{iso} = -1284.7$, $\delta_{aniso} = -334$, and $\eta = 0.1$, which were determined from a ^{117}Sn MAS NMR spectrum (see Figure 10). Zero asymmetry parameters η are found when the tin atoms have a point group with a 3-fold axis element or higher. Slight distortions as in the structure of β-SnB_4O_7 result in small but nonzero asymmetry parameters.

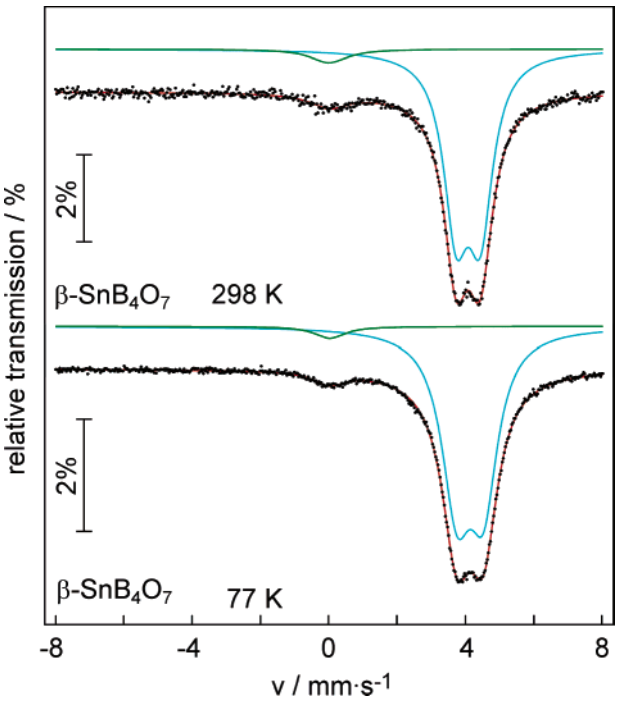

Figure 9. Experimental and simulated ^{119}Sn spectra of β-SnB_4O_7 at 77 K and room temperature.

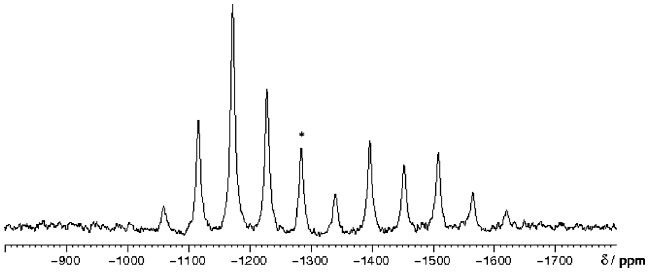

Figure 10. ^{117}Sn MAS NMR spectrum of β-SnB_4O_7; all peaks can be explained by a single tin position ($\delta_{iso} = -1284.7$, $\delta_{aniso} = -334$, $\eta = 0.1$); the isotropic sideband is marked by an asterisk.

Table 9. Fitting Parameters for the ^{119}Sn Mössbauer Spectra of β-SnB_4O_7 at Room Temperature and 77 K[a]

T (K)	δ_1 (mm s^{-1})	Γ_1 (mm s^{-1})	ΔE_Q (mm s^{-1})	δ_2 (mm s^{-1})	Γ_2 (mm s^{-1})
298	4.09(1)	0.88(1)	0.71(3)	0.01(1)	1.3(1)
77	4.14(1)	1.06(1)	0.78(3)	0.03(3)	1.1(1)

[a] δ = Isomer shift; Γ = experimental line width; ΔE_Q = electric quadrupole interaction. For details, see text.

Because the high-pressure phase β-SnB_4O_7 is an extreme example for a highly coordinated tin atom, we compared the observed chemical shift parameters with literature values.[84−89] Prior work[88,89] on thiostannates indicates that it is impossible to distinguish Sn^{2+} and Sn^{4+} on the basis of $^{117/119}$Sn NMR because of the mutual overlap of anisotropic and isotropic chemical values for Sn^{2+} and Sn^{4+}. In fact, the situation is more favorable for tin coordinated to oxygen. The values of the anisotropic and isotropic chemical shifts span a space in which Sn^{2+} and Sn^{4+} atoms are well-separated from each other (Figure 11). Obviously, the

(77) Ren, M.; Lin, J. H.; Dong, Y.; Yang, L. Q.; Su, M. Z.; You, L. P. *Chem. Mater.* **1999**, *11*, 1576−1580.
(78) Laperches, J. P.; Tarte, P. *Spectrochim. Acta* **1966**, *22*, 1201−1210.
(79) Blasse, G.; van den Heuvel, G. P. M. *Phys. Status Solidi A* **1973**, *19*, 111−117.
(80) Steele, W. C.; Decius, J. C. *J. Chem. Phys.* **1956**, *25*, 1184−1188.
(81) Böhlhoff, R.; Bambauer, H. U.; Hoffmann, W. *Z. Kristallogr.* **1971**, *133*, 386−395.
(82) Machida, K.; Hata, H.; Okuno, K.; Adachi, G.-Y.; Shiokawa, J. *J. Inorg. Nucl. Chem.* **1979**, *41*, 1425−1430.
(83) Lippens, P. E. *Phys. Rev.* **1999**, *B 60*, 4576−4586.

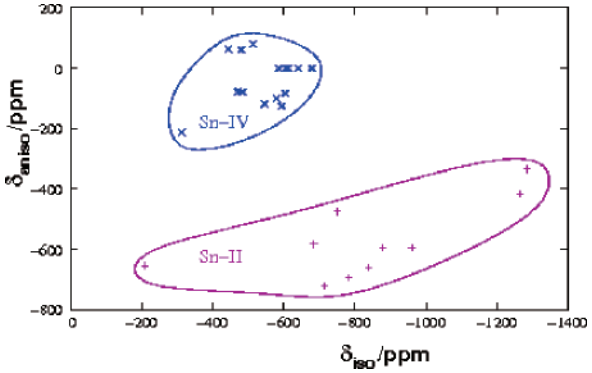

Figure 11. Chemical shift parameters of Sn^{2+} and Sn^{4+} in oxygen-based, crystalline model compounds (refs 84−87 and β-SnB_4O_7); some δ_{aniso} values were too small to be determined experimentally and were assumed to be zero for this diagram.

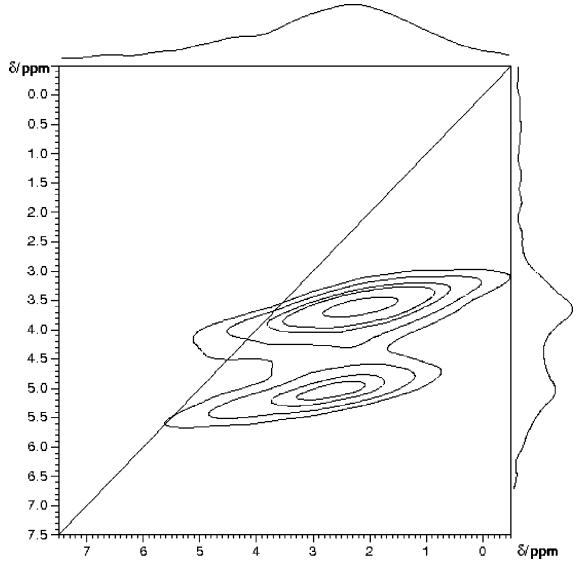

Figure 12. ^{11}B MQMAS NMR spectrum of crystalline β-SnB_4O_7; two crystallographically independent positions are resolved (δ_{iso} = 3.4 and 4.6, SOQE = 0.7 and 1.1 MHz, respectively).

chemical shift parameters of thiostannates are much more difficult to understand, because of the higher electronic polarizability of sulfur compared to oxygen. The resolution power of $^{117/119}Sn$ MAS NMR experiments might be useful in determining oxidation states spectroscopically in various amorphous and crystalline inorganic materials.

From the ^{11}B MQMAS (Figure 12), the chemical shift and quadrupole coupling parameters were determined to be δ_{iso} = 3.4 and 4.6 and SOQE = 0.7 and 1.1 MHz, respectively. The determined SOQE and the isotropic chemical shift parameters are typical for tetrahedrally coordinated boron atoms.[90]

Conclusions

Implementing a high-pressure/high-temperature strategy, we synthesized and characterized the crystalline compound β-SnB_4O_7 in the system Sn−B−O, in which previously only glasses were known. This new approximand of the glassy state enabled us to put up a correlation of the oxidation state of tin atoms coordinated to oxygen atoms with the $^{117/119}Sn$ chemical shift on the basis of isotropic and anisotropic chemical shift parameters.

Generally, one would expect that the nucleation and growth of a crystalline phase from the amorphous "SnB_4O_7" with increasing pressure is impeded by a suppressed ionic mobility at higher pressures. Hence, under synthetic conditions of 7.5 GPa and 1100 °C, we presume a high ionic mobility, as the different experiments always resulted in crystalline β-SnB_4O_7, even when the sample was quenched to room temperature. These observations suggest that the reconstructive formation of the more densely packed compound β-SnB_4O_7 under pressure is kinetically not restricted at a temperature of 1100 °C.

Our strategy was successfully applied in the systems Hf−B−O and Zr−B−O. Both systems revealed no ternary crystalline borates up to the start of our synthetic investigations. The pressure of 7.5 GPa in combination with a temperature of 1200 °C led to the synthesis of the new crystalline compounds β-HfB_2O_5[91,92] and β-ZrB_2O_5.[93] These examples accentuate the great significance of high-pressure/high-temperature synthesis for the knowledge of crystalline approximands in glass-forming systems.

Acknowledgment. We thank Thomas Miller for collecting the single-crystal data, Dipl. Chem. Bettina V. Lotsch for the in situ powder diffraction measurements, Dipl. Chem. Andreas Sattler for the DTA/TG measurements, Christian Minke (LMU München) for technical support, and Priv.-Doz. Dr. Lorenz Kienle (MPI Stuttgart) for the electron diffraction experiments. Special thanks to Priv.-Doz. Dr. Petra Becker, Dr. L. Bayarjargal, and Prof. Dr. L. Bohatý (Universität zu Köln) for help with powder SHG measurements. We also thank Prof. Dr. W. Schnick (LMU München) for the continuous support of these investigations. This work was financially supported by the Deutsche Forschungsgemeinschaft (HU 966/2-2) and the European Science Foundation within the COST D30 network (D30/003/03).

Supporting Information Available: Crystallographic information (CIF). This material is available free of charge via the Internet at http://pubs.acs.org.

CM061946W

(84) Amornsakchai, P.; Apperley, D. C.; Harris, R. K.; Hodgkinson, P.; Waterfield, P. C. *Solid State Nucl. Magn. Reson.* **2004**, *26*, 160−171.
(85) Cruz, L. P.; Savariault, J.-M.; Rocha, J.; Jumas, J.-C.; Pedrosa de Jesus, A.; Pedrosa, de Jesus, J. D. *J. Solid State Chem.* **2001**, *156*, 349−354.
(86) Cossement, C.; Darville, J.; Gilles, J.-M.; Nagy, J. B.; Fernandez, C.; Amoureux, J.-P. *Magn. Reson. Chem.* **1992**, *30*, 263−270.
(87) Mackenzie, K. J. D.; Smith, M. E. *Multinuclear Solid-State NMR of Inorganic Solids*; Pergamon: Amsterdam, 2002.
(88) Mundus, C.; Taillades, G.; Pradel, A.; Ribes, M. *Solid State Nucl. Magn. Reson.* **1996**, *7*, 141−146.
(89) Pietrass, T.; Taulelle, F. *Magn. Reson. Chem.* **1997**, *35*, 363−366.
(90) Kroeker, S.; Stebbins, J. F. *Inorg. Chem.* **2001**, *40*, 6239−6246.
(91) Huppertz, H.; Knyrim, J. S. *Acta Crystallogr., Sect. A* **2006**, *62*, s59.
(92) Knyrim, J. S.; Huppertz, H. *J. Solid State Chem.* **2007**, in press.
(93) Knyrim, J. S.; Huppertz, H. unpublished results.